Tetragonal phase stability maps of ceria-yttria co-doped zirconia: From powders to sintered ceramics

Peyman Khajavi, Yu Xu, Henrik Lund Frandsen, Jérome Chevalier, Laurent Gremillard, Ragnar Kiebach, Peter Vang Hendriksen

Tetragonal phase stability maps of ceria-yttria co-doped zirconia: from powders to sintered ceramics

Published in Ceramics International 46 [7] (2020), pp. 9396-9405

https://doi.org/10.1016/j.ceramint.2019.12.199

Peyman Khajavi[1,*], Yu Xu[1], Henrik Lund Frandsen[1], Jérôme Chevalier[2], Laurent Gremillard[2], Ragnar Kiebach[1], Peter Vang Hendriksen[1]

1. Department of Energy Conversion and Storage, Technical University of Denmark, Frederiksborgvej 399, 4000 Roskilde, Denmark
2. Univ Lyon, INSA-Lyon, CNRS, MATEIS UMR 5510, F-69621 Villeurbanne, France

* Corresponding author: kha@dtu.dk

Abstract

Ceria-Yttria co-doped tetragonal zirconia is an attractive class of materials having high strength, toughness and thermal stability. In this study, several co-doped zirconia powders with different stabilizers contents were synthesized via continuous hydrothermal flow synthesis (CHFS). The CHFS was concluded as a suitable method in synthesizing ultrafine tetragonal zirconia particles with controlled morphology. The synthesized powders as well as some commercial powders were heat-treated both in the form of powders and pellets between 1150 and 1500°C and their crystalline structure after cooling to room temperature was studied. The results were used to map out the stability range of the tetragonal phase. The developed diagrams are useful tools to select the appropriate amounts of stabilizers applicable for different sintering temperatures and for samples with different target densities.

Keywords

Tetragonal zirconia, Ceria, Yttria, Phase diagram, Toughness

1. Introduction

Tetragonal zirconia is a widely studied and technologically important material due to its wide range of applications from structural and engineering ceramics to catalytic materials. Superior mechanical properties of tetragonal zirconia have made it an interesting structural ceramic for use in solid oxide fuel and electrolysis cells, membranes, and biomedical applications [1–7].

In pure zirconia, under certain conditions, the tetragonal crystalline phase can be maintained at room temperature, in a metastable form. The metastable tetragonal form can be fully retained while being calcined at temperatures in the range of 400-800°C. However, further increase in the temperature will result in a tetragonal to monoclinic phase transformation during subsequent cooling [8–12]. The phase transformation entails a volume expansion and a shear strain of approximately 4 and 16%, respectively [13].

For most engineering applications the component manufacturing process includes sintering at high temperatures, usually above 1100°C. Consequently, in practice to retain the tetragonal phase, zirconia is doped with certain amounts of stabilizing element(s). The stabilizer content should be high enough to preserve the tetragonal phase upon cooling from a high sintering temperature. This prevents undesired volumetric expansion from spontaneous transformation to the monoclinic zirconia, which could result in formation of micro-cracks having detrimental effect on the mechanical properties of the component. Furthermore, the stabilizer content should not be too high, as it over-stabilizes the tetragonal phase, thus inhibits transformation toughening [14–18]. The transformation toughening mechanism occurs when the stress field around a propagating crack initiates a stress-induced martensitic tetragonal to monoclinic phase transformation. The volume increase associated with the transformation leads to extra work (dissipation of energy) associated with the crack propagation and consequently to a tougher material. Thus, the stabilizer content should be close to a certain critical amount, for a specific grain size, to increase the transformability of the material and make it prone to undergo the transformation with the stress field at the crack tip [13,19,20].

To summarize; in order to benefit the most from the transformation toughening mechanism, two important properties should be carefully balanced; the meta-stability of the tetragonal phase and its transformability. Optimum strength and fracture toughness is achieved when the tetragonal zirconia is maintained after sintering and cooling but the phase is not over-stabilized (preventing transformation toughening, which is a function stabilizer content and grain size) [18,21,22].

The right amount of stabilizer can be difficult to choose, as it is influenced by several factors such as packing density, grain size, and sintering temperature. For example, the tendency for the tetragonal to monoclinic transformation is higher in porous bodies (for example used as the support component for solid oxide fuel and electrolysis cells and membranes, where a porosity of more than 35% is typically desirable) than in fully dense ceramics for which most investigations have been carried out [23,24]. Nanocrystalline structures are another example; they have the potential for achieving a high toughness by decreasing the stabilizer content, since the small grain size, initially and after sintering, can inhibit loss of the tetragonal phase [25]. However, a significantly lower fracture toughness is also reported in literature for nanostructured stabilized zirconia ceramics as compared to larger grained zirconia. The reason has been attributed to a lower transformability of the smaller grains [26,27]. Another factor to consider is the amount of monoclinic or cubic phases that form during manufacturing, as these take up space for tetragonal crystals thereby decreasing the number of grains active for the stress-induced transformation.

Yttria and ceria stabilized tetragonal zirconia (Y-TZP and Ce-TZP) have been widely studied and used due to their excellent mechanical properties [13,22]. Compared to Y-TZP, Ce-TZP has a

higher toughness but a lower strength. Moreover, Ce-TZP is less prone to low temperature degradation (LTD) [16,18,28]. Therefore, co-doping with Y and Ce is a promising route to optimize strength, toughness and thermal stability of TZP ceramics [29–37]. Lin and co-workers [33–35] studied the mechanical properties of ceria-yttria co-doped zirconia ceramics sintered at 1500°C containing different amounts of stabilizers. They concluded that CeO_2 and $YO_{1.5}$ contents of 6.5-7 mol% and 2.25-3 mol%, respectively, were the optimum amounts giving the highest toughness and strength. Duh and co-workers [29] reported a very high toughness for the zirconia ceramic stabilized with 5.5 mol% CeO_2 and 2 mol% $YO_{1.5}$ sintered at 1500°C, among different studied compositions. Duh and co-workers [31] reported that ceramic with 10 mol% CeO_2 and 1 mol% $YO_{1.5}$ sintered at 1500°C was the toughest material; however, the studied materials had considerable amounts of monoclinic phase after sintering. Accordingly, from literature it is difficult to determine conclusively the range of stabilizers providing the optimum strength and toughness for the Ce-Y co-doped ceramics.

For porous structures, the typical lower sintering temperatures makes it possible to decrease the stabilizer content without experiencing spontaneous tetragonal to monoclinic phase transformation on cooling, and thus to gain further strength and fracture toughness. On the other hand, the stability of the tetragonal phase in a porous body is lower than that in a dense structure. Therefore, it is important to understand the dependency of the stability of the tetragonal phase on sample density and sintering temperatures. There is however a lack of studies on appropriate Ce-Y stabilizer contents optimizing strength and toughness in porous systems, especially when using low sintering temperatures, i.e. below 1200°C. Although some works have studied the equilibrium phase diagram data using thermodynamic calculations [38–40], the metastable phase diagrams of ZrO_2–Y_2O_3–CeO_2 system are rare in literature. Moreover, stabilized zirconia powders especially in the nanocrystalline form, often show different metastable tetragonal phase stability behavior compared to the equilibrium bulk phase diagram data [41–43], so it is necessary to study the stability ranges of the metastable tetragonal zirconia when varying sintering temperature and particle packing (density) in Ce-Y co-doped zirconia.

Consequently, the objective of this work is to map out the stable domains, in terms of stabilizer content and sintering temperatures, for the tetragonal Ce-Y co-doped zirconia in both porous and dense states. We have thus investigated different Ce-Y co-doped nanocrystalline zirconia powders *and* pellets with compositions ranging from 0 to 6% $YO_{1.5}$ and 0 to 7% CeO_2 at three different sintering temperatures, i.e. 1150°C, 1350°C and 1500°C. After heat treatment, the phase composition of the samples was investigated to identify the optimum amount of stabilizer at the specific sintering temperature. The results are used to construct transformation phase diagrams applicable for different porosities and heat-treatment temperatures (as required for the specific component targeted).

2. Experimental

2.1. Materials

Table 1 presents the compositions of the samples studied in this work. The samples are denoted as *m*Ce *n*Y-SZ, where *m* and *n* signify the content of CeO_2 and $YO_{1.5}$ in mol%, respectively and SZ stands for 'Stabilized Zirconia'.

Ce-Y co-doped nanocrystalline zirconia powders of six compositions were synthesized by Continuous Hydrothermal Flow Synthesis (CHFS) using an in-house developed two-stage reactor [44]. $ZrO(NO_3)_2{\cdot}xH_2O$ (with $x{\sim}1$), $Y(NO_3)_3{\cdot}6H_2O$ and $Ce(NO_3)_3{\cdot}6H_2O$ (Sigma Aldrich) and KOH (Alfa Aesar) were used as the raw materials.

The as-received zirconium, yttrium and cerium salts were first dissolved separately in DI water to prepare the "stock solutions". To ascertain the cation concentrations of the prepared solutions, ca. 5 gr of each solution was calcined in a muffle furnace in air at 900°C for 6 h in order for the salt to be fully converted to the corresponding metal oxide. By measuring the weight of the samples before and after the calcination the concentration of the cations in the initial solutions was established. Later, these stock solutions were diluted and mixed to prepare the aqueous "precursor solution" for the powder syntheses.

Table 1: The samples studied in this work; the sample composition is designated mCe nY-SZ.

Supplier	Ce mol% (*m*)	Y mol% (*n*)
Synthesized in this work (CHFS)	3	3
	4.5	1.5
	2.5	2.5
	5.5	2.5
	7	0
	6	1
Cerpotech	4	1
	4.5	1.5
	5	2
	0	4.6
Tosoh	0	4
	0	5
	0	6
Nanoe	1.5	4.5
	3	3.6
	5	3

The precursor solution for each specific composition was prepared considering the stoichiometric molar ratios of yttrium, cerium and zirconium. A total cation concentration of 0.05 mol/L was applied for the solutions. Aqueous alkali solutions with a concentration of 1 mol/L were also prepared by dissolving KOH pellets in DI water and used as "mineralizer" in the syntheses. Syntheses pressure and temperature were 27 MPa and 683 K, respectively.

To extend the range of the studied compositions, ten different Y doped and Ce-Y co-doped zirconia compositions were also purchased from external suppliers (Tosoh, Japan; Nanoe, France; Cerpotech, Norway). For comparison with the synthesized powders, one of the purchased compounds was such chosen to have a similar composition as one of the synthesized powders (see Table 1).

Some of the powders were pressed into pellets by a uniaxial press (200 MPa) and further densified using cold isostatic pressing (4 GPa). The two set of samples (powders and pellets) were heat treated for 2 h in air at 3 different temperatures; 1150, 1350, and 1500°C, with a heating and cooling rate of 90 °C/h.

2.2. Characterization

X-ray diffraction (XRD) was performed using a Bruker D8 diffractometer (Bruker, Germany) with Cu Kα radiation. The diffraction patterns of all samples were recorded over three different 2θ ranges. A wide scan was first carried out over the 10-90° range with step size and scan speed of 0.03° and 0.015°/s, respectively. Two high-resolution scans with step size and scan speed of 0.003° and 0.0015°/s were also performed over the ranges of 25.5-33.5° and 70.5-76.5° to identify precisely the presence of monoclinic and cubic phases in the samples.

When no cubic phase was detected in the samples (from the high-resolution scans over 70.5-76.5°), the volume fractions of the tetragonal and monoclinic phases (V_t and V_m) were evaluated from the integrated peak intensities, I, of the $(101)_t$, $(111)_m$ and $(\bar{1}11)_m$ planes using the method developed by Toraya et al. [45]

$$X_m = \frac{I_m(111) + I_m(\bar{1}11)}{I_m(111) + I_m(\bar{1}11) + I_t(101)} \quad (1)$$

$$V_m = \frac{1.311X_m}{1 + 0.311X_m} \quad (2)$$

$$V_t = 1 - V_m \quad (3)$$

The subscripts m and t represent the monoclinic and tetragonal polymorphs, respectively.

The average crystallite size of the tetragonal phase (d) in the synthesized samples was estimated from the $(101)_t$ diffraction peak using the Scherrer equation [46],

$$d = \frac{K\lambda}{\beta cos\theta} \quad (4)$$

where K is the shape constant (≈ 0.9), λ is the radiation wavelength, θ is the diffraction peak angle and β is the corrected full width at half-maximum intensity (FWHM). A NIST standard silicon powder was used as a standard to correct for the instrumental broadening. XRD data were also analyzed through the Rietveld refinement method [47] using the WINPOW, a modified version of

the LHMP program [48]. The background and peak profiles were fitted using Chebyshev polynomials and Pseudo-Voigt functions, respectively.

For samples containing the cubic phase, the crystalline phase composition was determined using the Rietveld refinement.

The morphology of the CHFS powders was studied with a JEOL 3000F transmission electron microscope with a field emission gun operating at 300 kV. The particles were dispersed in ethanol by means of ultrasonic treatment and dropped onto a holey carbon film/Cu grid.

The specific surface area of the pristine (starting) and calcined powders was measured using the Brunauer-Emmett-Teller (BET) method [49] on a Quantachrome surface area analyzer (Quantachrome, USA). Assuming that the powders are composed of monodispersed and spherical particles, the average particle sizes of the powders were estimated from their BET surface area (S_{BET}) and density (ρ) using the following equation [50]:

$$d_{BET} = \frac{6}{S_{BET}\,\rho} \tag{5}$$

Density of the sintered pellets was determined using their weight and geometric volume.

Microstructure of the sintered pellets was studied using field emission scanning electron microscopy (FE-SEM, Zeiss Merlin, Germany). The samples were polished and then thermally etched at 1150°C for 15 min with a heating and cooling rate of 250 °C/h. The average grain size of each sample was determined by measuring the size of ca. 100 grains.

3. Results and discussion

3.1. Morphology of the synthesized powders

Figure 1a, b show high resolution TEM images of the as-synthesized 5.5Ce 2.5Y-SZ powder. The nanoparticles have a nearly spherical morphology and display a monodisperse particle size distribution with an average size of 8.6 nm (standard deviation 1.6 nm) determined by measuring the diameter of 60 particles. Moreover, the particles are fully crystallized. From the higher magnification image (Figure 1b**)** the interplanar spacing and the angle between planes are measured to be 2.97 Å, 2.60 Å, 1.82 Å and 55°, which is consistent with the (101), (002), (112) planes and ∠[(101)/(002)] of a tetragonal crystal. For comparison, the calculated interplanar spacing of the crystal planes of the tetragonal 5.5Ce 2.5Y-SZ on basis of lattice parameters derived from the Rietveld refinement of the XRD data are provided in the appended Supporting Information.

Figure 2a is a micrograph of a particle from the 5.5Ce 2.5Y-SZ powder after calcination at 1500°C. The particle size has markedly increased due to sintering of the primary nanosized particles. The sintering effect is more clearly observed in the high-resolution image (Figure 2b), showing a distinguishable grain boundary in the particle. The particle is polycrystalline with randomly-oriented grains (Figure 2c).

The CHFS, as a type of high-throughput synthesis technique, is thus well suited for synthesizing very fine, monodisperse crystalline zirconia particles in a continuous and efficient synthesis process.

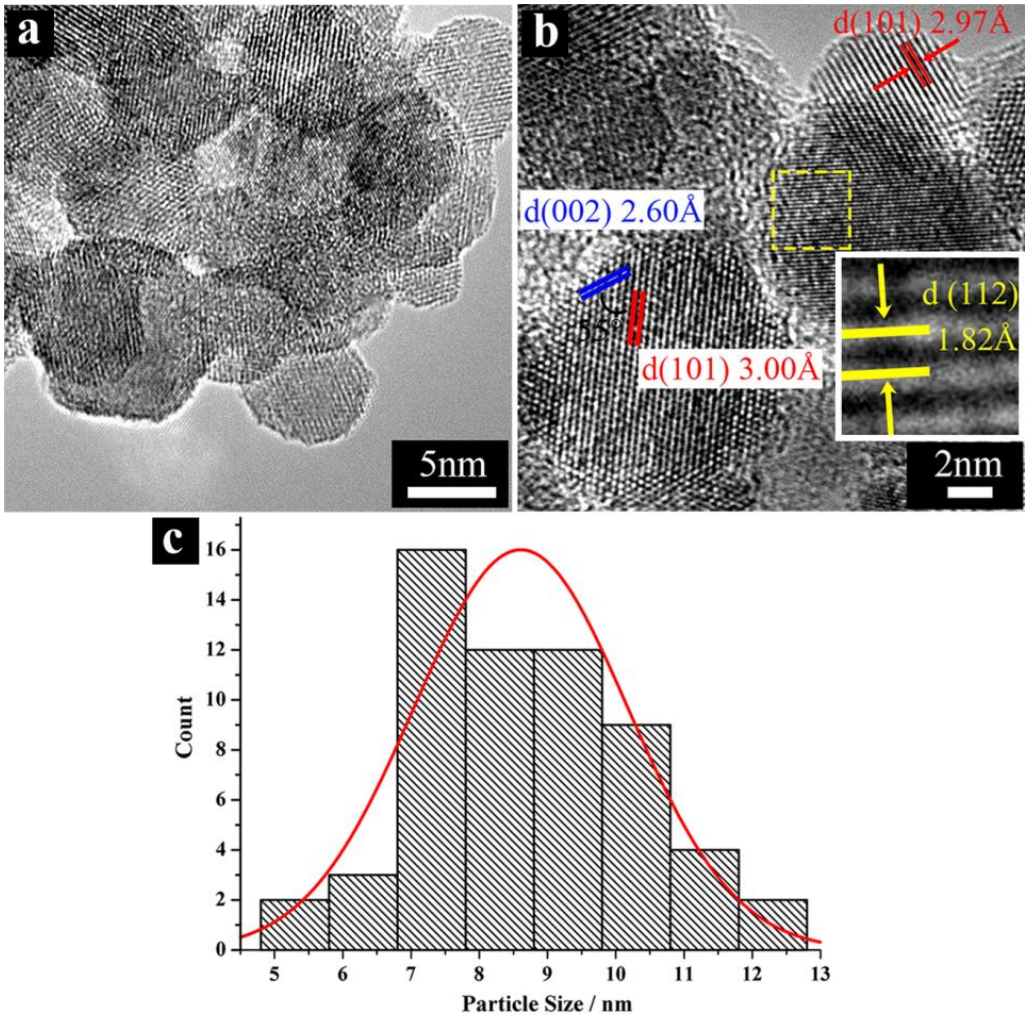

Figure 1: (a, b) high-resolution TEM micrographs of the as-synthesized 5.5Ce 2.5Y-SZ nanoparticles and (c) the particle size distribution determined from the diameter of 60 particles. The higher magnification micrograph (b) shows visible lattice fringes that are attributed to crystal planes based on the measured interplanar spacing. The inset provides a zoom-in view of the lattice fringe (highlighted by the dashed square) for a better readability.

3.2. Crystalline phase of the synthesized powders

The XRD patterns of the as-synthesized powders (Figure 3) show that these are all crystalline. The crystallite sizes of the powders, measured from the XRD results, are also presented in Figure 3. The 8.1 nm crystallite size determined for the 5.5Ce 2.5Y-SZ powder is in a good agreement with the particle size measured by TEM (8.6 nm).

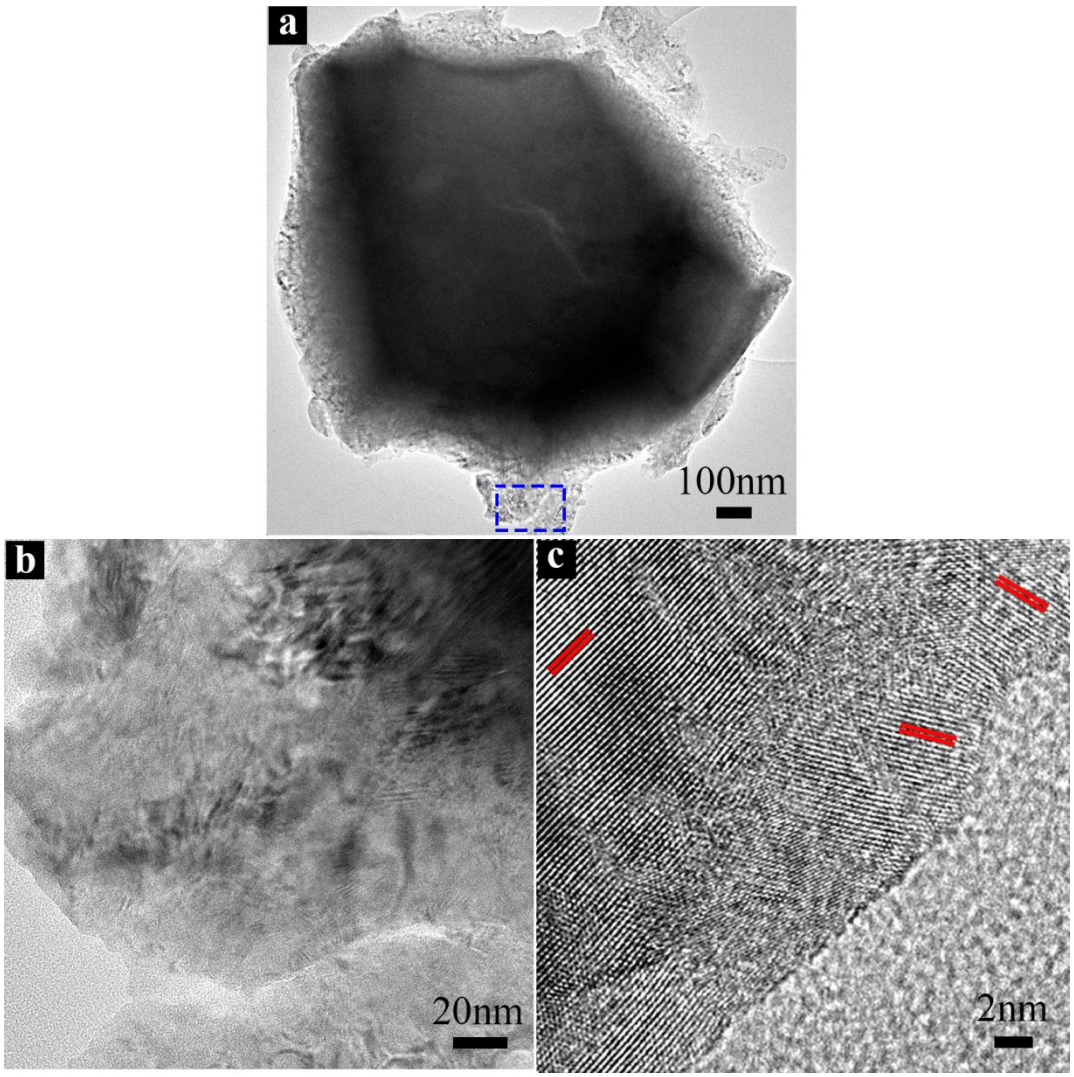

Figure 2: (a) BF-TEM micrograph of a calcined 5.5Ce 2.5Y-SZ particle (b) BF-TEM micrograph of the highlighted area in (a), and (c) High-resolution image of an area in the calcined particle. The measured interplanar spacing (2.97 Å) matches well to the (101) plane of the tetragonal crystal.

The high-resolution scans over the 70.5-76.5° range (inset, Figure 3) show that all the powders are tetragonal. However, peaks for the (400) and (004) tetragonal planes are not well separated, and whether the (400) peak of the cubic phase is present or not is not well discernible. The question is thus if a small amount of cubic phase is present in the samples. It is in general difficult to distinguish between cubic and tetragonal phases from the XRD pattern of a nanocrystalline zirconia, as the inherent strong peak broadening causes peak overlap. It is reported in some studies that the cubic phase can also be stabilized at room temperature in pure zirconia powders having ultrafine crystallites, i.e. in the range of 2-20 nm [51–54]. Doping with stabilizers as done here, might well increase the possibility of forming the cubic phase. Considering the very small crystallite size of the powders

synthesized in this work, the possible presence of small amounts of the cubic phase was further investigated by the Rietveld refinement analysis [55] of the XRD data for one specific composition. The as-synthesized 5.5Ce 2.5Y-SZ powder, having high content of stabilizers (and hence most susceptible to formation of the cubic phase) was chosen for the analysis.

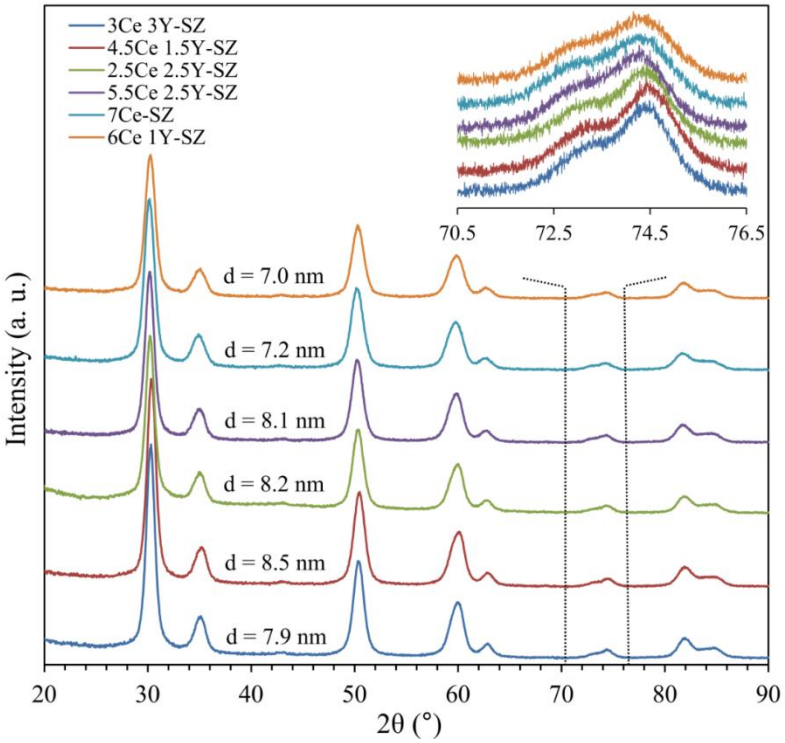

Figure 3: XRD patterns of the as-synthesized CHFS nanopowders; the inset shows the high-resolution scans within the range of 70.5°-76.5°.

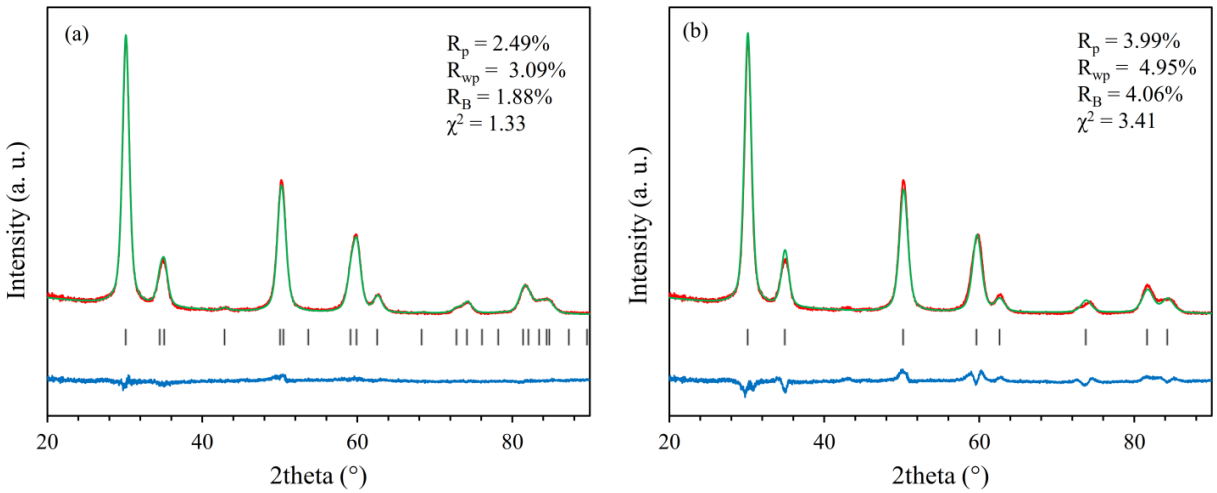

Figure 4: Rietveld refinement profiles of the XRD data for the as-synthesized 5.5Ce 2.5Y-SZ powder, refined based on (a) the tetragonal and (b) the cubic structures. The red and green lines represent the observed and calculated intensities, respectively. Bragg positions are indicated by the verticals. The difference curves are plotted by the blue lines. The refinement parameters are also presented for each set of refinement.

First, the refinement was carried out for the tetragonal and cubic phases individually. Figure 4presents the Rietveld refinement plots based on the tetragonal and cubic phases together with the corresponding goodness of fit (GoF) and reliability factors. A much better fitting, i.e. matching between the observed and calculated intensities, was achieved when the pattern was fitted with the tetragonal phase than with the cubic structure. This could also be concluded by comparing the refinement parameters of the two sets of analysis, where smaller R-factors and a GoF closer to unity are only obtainable for the tetragonal structure.

In addition, the Rietveld refinement was performed to investigate the presence of mixed tetragonal-cubic polymorphs. Here, the amount of cubic phase was concluded to be very low, i.e. less than 0.1%, after finishing the refinement. The results of the Rietveld refinement studies thus show that the as-synthesized powders are in the tetragonal phase, which is consistent with the HRTEM results of the 5.5Ce 2.5Y-SZ powder.

3.3. Specific surface areas of the powders

The BET specific surface area of selected powders, pristine and after calcination at 1150°C, is shown in Table 2. For each set of powders, at least one compound is investigated. The as-synthesized CHFS powder has the highest surface area, significantly higher than the other pristine samples. This is consistent with the ultrafine morphology of the CHFS powders as discussed earlier. The other pristine samples have comparable surface areas. In the calcined form, the surface area of the powders ranges between 0.5 – 5.9 m^2/g. The estimated average particle size of the calcined powders determined from their BET surface areas and the average crystallite size of their tetragonal and monoclinic phases measured from XRD are also presented in Table 2. The calcined powders (in particular CHFS powder) are composed of big agglomerates of smaller grains.

Table 2: BET specific surface area (S_{BET}), BET particle size (d_{BET}), and the average crystallite size of the tetragonal (d_t) and monoclinic (d_m) phases estimated using XRD patterns

Supplier	Compound	Pristine powder		Calcined at 1150°C			
		S_{BET} (m^2/g)	d_{BET} (nm)	S_{BET} (m^2/g)	d_{BET} (nm)	d_t (nm)	d_m (nm)
CHFS	4.5Ce 1.5Y-SZ	102.6	10	0.5	2004	26.3	25.4
Cerpotech	4Ce 1Y-SZ	10.3*	97	-	-	-	47.7
	4.5Ce 1.5Y-SZ	12.3*	81	5.9	173	69.5	44.1
	5Ce 2Y-SZ	13*	76	-	-	53.2	-
	4.6Y-SZ	10.3*	97	-	-	53.6	-
Tosoh	4Y-SZ	12.7	80	4.9	208	53.2	35.5
Nanoe	1.5Ce 4.5Y-SZ	20	51	2.4	412	52.8	-

* Reported by the supplier
- not analyzed/not applicable

3.4. Tetragonal phase stability maps

The crystalline phase compositions of all the studied powders after calcination at 1150, 1350, and 1500°C are tabulated in Table 3. For the 4.5Ce 1.5Y-SZ compound, the powder synthesized in this work and the purchased powder have very close phase compositions after calcination at all temperatures. The similar phase compositions and comparable crystallite sizes of these two powders despite their different extent of agglomeration (Table 2) suggest that the trend in the tetragonal to monoclinic phase transformation in the synthesized and purchased powders can be assumed similar. In other words, the phase transformation is more dependent on the stabilizer content than the preparation method of the starting powders in this case.

Density of the sintered pellets is also presented in Table 3. The density of pellets sintered at 1150°C varies between 60 – 80 % with the highest density pertinent to the pellets made of CHFS powder. This corresponds well with the very high surface area of its starting powder. The density of the pellets sintered at 1350 and 1500°C ranges between 80 – 100 %.

The amount of retained tetragonal phase for each compound is also presented in Figure 5a-c. Using these results, the tetragonal to monoclinic phase transformation boundaries for powders calcined at the three studied calcination temperatures can be developed, as shown by the dashed lines in Figure 5.

From thermodynamic analysis and assuming that the tetragonal crystallites fully transform to the monoclinic crystallites and not partially [56–58], the critical crystallite size (i.e. the size above which the tetragonal to monoclinic phase transformation occurs spontaneously) for the tetragonal to monoclinic phase transformation for unconstrained zirconia particles (D_c) at a given temperature (T) can be expressed as:

$$D_c = -6\,\frac{\Delta\sigma}{q\,(1-\frac{T}{T_b})} \qquad (6)$$

where $\Delta\sigma$ is the difference between surface free energy of the tetragonal and monoclinic phases, q is the enthalpy of the tetragonal to monoclinic phase transformation and T_b is the transformation temperature, all defined for a crystal with infinite size.

For a constrained system, the critical grain size for the transformation (D_c^*) is obtained considering the difference between interfacial energy of the tetragonal and monoclinic phases ($\Delta\sigma^*$) and strain energy difference of the two phases ($\Delta\epsilon$):

$$D_c^* = -6\,\frac{\Delta\sigma^*}{q\,\left(1-\frac{T}{T_b}\right)+\Delta\epsilon} \qquad (7)$$

Equations (6) and (7) suggest that for a certain composition the critical grain size in a bulk solid material (constrained state) is larger than the critical crystallite size in the powder form (unconstrained state), resulting from the contribution of the strain and interfacial energies in the constrained state. This is in good agreement with experiments [59]. For instance, the critical crystallite size for stabilizing the tetragonal phase at room temperature for 0.5YSZ (0.5mol% yttria doped zirconia), 1YSZ and 1.5YSZ powders has been reported to be 30, 51, and 71 nm, while in the constrained solid state, the corresponding critical grain size for each composition is found to be 70, 100 and 155 nm [59].

The contribution of the strain energy to stabilize the tetragonal phase is dependent on its magnitude. The extent of the strain energy decreases by increasing the porosity of the solid, as the

pores provides free surfaces and lowers the elastic modulus [60]. As a consequence, more grains in a porous body will have the opportunity to transform to the monoclinic phase upon cooling. For instance, Lange [60] reported the amount of tetragonal phase retained at room temperature in 2.5 mol% yttria doped zirconia sintered at 1500°C to be 97, 83, and 77% for relative densities of 92, 73, and 65%, respectively.

Therefore, the developed diagrams based on the calcined powders in Figure 5are not descriptive for dense sintered bodies. To consider the effects of matrix constraint, the transformation boundary diagrams were completed using the crystalline phase analysis results of sintered pellets. The powders, in which the high temperature tetragonal phase could not be fully retained after cooling to room temperature, were further investigated in the pellet form. The crystalline phase composition of the pellets sintered at 1150, 1350, and 1500°C is also provided in Table 3 (in brackets) and in Figure 5a-c. The transformation boundaries for the dense state at the three studied temperatures, derived from the results for the sintered pellets, are drawn in Figure 5 as solid lines. As expected the stability of the tetragonal phase in the pellets was higher than that in the powder due to the stabilizing effects of the matrix constraints in the solid form.

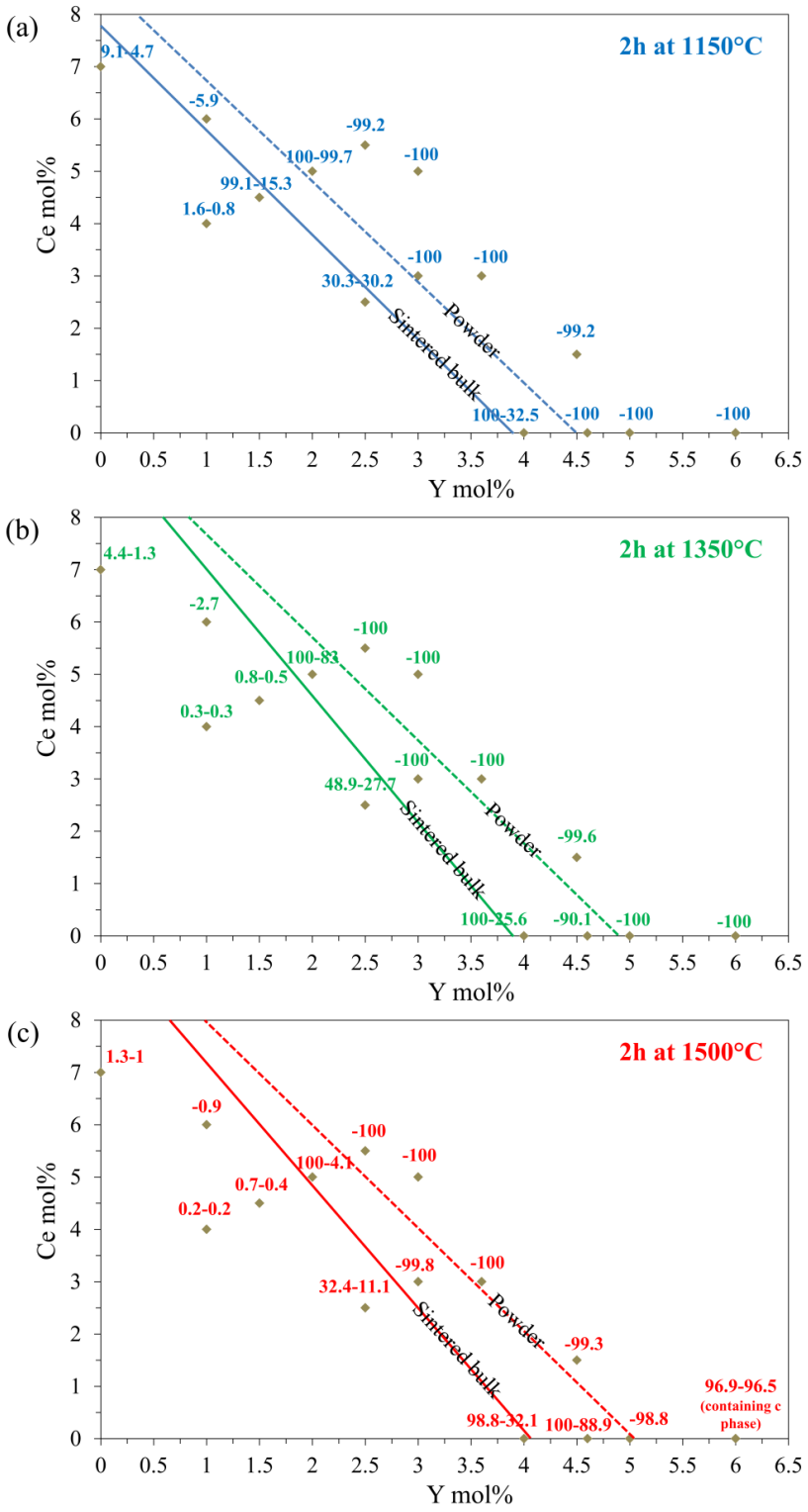

Figure 5: Amount of retained tetragonal phase for each compound in the form of powder (right number) and pellet (left number) after the heat treatment at (a) 1150°C, (b) 1350°C and (C) 1500°C. The dashed and solid lines indicate the approximate transformation boundary diagrams for calcined powders and sintered pellets, respectively.

Table 3: Crystalline phase composition of the calcined powders and sintered pellets and relative density (D) of the sintered pellets studied in this work. The phase composition of the sintered pellets is shown in the brackets. The uncertainty of the porosity measurements is around 1-2%.

		Samples heat-treated at 1150°C				**Samples heat-treated at 1350°C**				**Samples heat-treated at 1500°C**			
Supplier	**Compound**	**Phase composition**			***D* (%)**	**Phase composition**			***D* (%)**	**Phase composition**			***D* (%)**
		monoclinic	**tetragonal**	**cubic**		**monoclinic**	**tetragonal**	**cubic**		**monoclinic**	**tetragonal**	**cubic**	
CHFS	3Ce 3Y-SZ	0.0	100	0.0	-	0.0	100	0.0	-	0.2	99.8	0.0	-
	4.5Ce 1.5Y-SZ	82	18	0.0	-	97.8	2.2	0.0	-	98.8	1.2	0.0	-
	2.5Ce 2.5Y-SZ	69.8 [69.7]	30.2 [30.3]	0.0 [0.0]	81	72.3 [51.1]	27.7 [48.9]	0.0 [0.0]	90.6	88.9 [67.6]	11.1 [32.4]	0.0 [0.0]	95.7
	5.5Ce 2.5Y-SZ	0.8	99.2	0.0	-	0.0	100.0	0.0	-	0.0	100.0	0.0	-
	7Ce-SZ	95.3 [90.9]	4.7 [9.1]	0.0 [0.0]	78.5	98.7 [95.6]	1.3 [4.4]	0.0 [0.0]	90.1	99 [98.7]	1 [1.3]	0.0 [0.0]	94.5
	6Ce 1Y-SZ	94.1	5.9	0.0	-	97.3	2.7	0.0	-	99.1	0.9	0.0	-
Cerpotech	4Ce 1Y-SZ	99.2 [98.4]	0.8 [1.6]	0.0 [0.0]	63.5	99.7 [99.7]	0.3 [0.3]	0.0 [0.0]	84.3	99.8 [99.8]	0.2 [0.2]	0.0 [0.0]	91.2
	4.5Ce 1.5Y-SZ	84.7 [0.9]	15.3 [99.1]	0.0 [0.0]	58.9	99.5 [99.2]	0.5 [0.8]	0.0 [0.0]	79.6	99.6 [99.3]	0.4 [0.7]	0.0 [0.0]	90.4
	5Ce 2Y-SZ	0.3 [0.0]	99.7 [100]	0.0 [0.0]	62	13 [0.0]	83 [100]	0.0 [0.0]	80.5	95.9 [0.0]	4.1 [100]	0.0 [0.0]	93.1
	4.6Y-SZ	0.0	100.0	0.0	-	9.9	90.1	0.0	-	11.1 [0.0]	88.9 [100]	*	94.8
Tosoh	4Y-SZ	67.5 [0.0]	32.5 [100]	0.0 [0.0]	70.9	74.4 [0.0]	25.6 [100]	0.0 [0.0]	98	67.9 [0.2]	32.1 (98.8)	0.0 [0.0]	99.1
	5Y-SZ	0.0	100.0	0.0	-	0.0	100.0	0.0	-	1.2	98.8	*	-
	6Y-SZ	0.0	100.0	0.0	-	0.0	100.0	*	-	0.0	96.5 [96.9]	3.5 [3.1]	97.8
NanoE	1.5Ce 4.5Y-SZ	0.8	99.2	0.0	-	0.4	99.6	0.0	-	0.7	99.3	*	-
	3Ce 3.6Y-SZ	0.0	100.0	0.0	-	0.0	100.0	0.0	-	0.0	100.0	0.0	-
	5Ce 3Y-SZ	0.0	100.0	0.0	-	0.0	100.0	0.0	-	0.0	100.0	0.0	-

* Negligible

As can be seen in Figure 5and Table 3, the retained tetragonal phase in the calcined powders typically decreases with increased calcination temperature. For instance, in the 5Ce 2Y-SZ compound the amount of tetragonal phase maintained at room temperature after calcination at 1150, 1350, 1500°C is 99.7, 83 and 4.1%, respectively. This trend can be attributed to the higher temperatures promoting grain growth to a size larger than the critical one. However, in some of the samples the amount of retained tetragonal phase increased or showed only little variation with increasing calcination temperature. For example, in the case of 4Y-SZ powder the amount of retained tetragonal phase after calcination at 1150, 1350 and 1500°C was 32.5, 25.6 and 32.1%, respectively.

In fact, by increasing the calcination temperature the degree of aggregation and crystallite size both increase. The former enhances the stability of the tetragonal phase, while the latter has a destabilizing effect. Hence, a possible explanation for the observed results in 4Y-SZ powder can be the stabilizing effect of the added constraint dominating the destabilizing effect of grain growth for the sample calcined at 1500°C. Confirming this hypothesis requires studying the evolution in crystallite size and degree of aggregation (or grain size and density level in the pellet form) during heat treatment, which is beyond the scope of this work.

The results indicate that the stability of the tetragonal phase is a complex function of stabilizer content, particle packing and sintering temperature (and dwelling time). The critical grain size for the tetragonal to monoclinic transformation depends not only on the composition (type and content of stabilizing agents) but also on sample density (i.e. the order of the constraint on transforming particles). Furthermore, the density might also have a destabilizing effect as increased density facilitates grain growth.

Equation (6) predicts the critical crystallite size for unstrained isolated crystals. However, in practice the critical crystallite size in the powder form may be different arising from the fact that the presence of hard agglomerates and/or aggregates will somewhat introduce a certain strain (also interfacial) energy. For pure zirconia nanopowders forming aggregates, Shukla and co-workers [8] found the critical diameter to be 41 nm, higher than the 10 nm calculated value for a single isolated particle, which is in good accordance with the reported experimental values [8,9]. Nanocrystalline powders are typically highly aggregated after heat treatment at high temperatures (e.g. as seen in Figure 2). The crystalline phase results of the studied powders in this work can thus be considered representative of solid ceramics with high porosities (> 50%).

Therefore, for each individual sintering temperature, the area between the corresponding dashed and solid lines in Figure 5demarcates the region, where the appropriate amounts of stabilizers can be chosen. For a dense system, the solid lines specify the lowest limit of stabilizers, where a further decrease in stabilizer(s) can cause losing the tetragonal grains upon cooling. For a porous system on the other hand, a higher amount of stabilizer should be utilized, as the tetragonal grains in a porous matrix can easier undergo the transformation. The appropriate amount of the Ce-Y stabilizers can approximately be shown by the dashed lines (concluded from the results of samples in the powder state). Here, a further increase will probably over-stabilize the tetragonal grains. The developed transformation phase diagrams thus take all the three effective parameters (density, stabilizer content and sintering temperature) into account.

From the developed transformation boundary diagrams, the slope of the dashed lines at the three studied temperatures is approximately equal to 2, showing that for a porous system the $YO_{1.5}$ stabilizer can be replaced with CeO_2 at twice the concentration. For a dense system, the solid lines have slightly different slopes, i.e. 2.1, 2.4, and 2.35 for heat treating at 1150, 1350, and 1500°C, respectively. Accordingly, the stabilizing effect of $YO_{1.5}$ can, as a rule of thumb, be considered twice

that of CeO_2. This difference in stabilizing efficiency can possibly be explained by considering the different stabilizing mechanisms of these two stabilizers.

The very small size of Zr^{4+} cations (0.84 Å) compared to O^{2-} onions (1.38 Å) is not ideal for the 8-fold oxygen coordination in fluorite structure (considering its minimum required cation-anion radius ratio of 0.732, *vs* 0.609 here). The resulting "oxygen overcrowding" around the Zr^{4+} cations makes the high temperature tetragonal and cubic phases unstable at room temperature. Doping aliovalent cations in the zirconia lattice can reduce this oxygen "overcrowding", consequently stabilizing the tetragonal (and cubic) zirconia. The stabilizing- mechanism(s) and efficiency of the dopant cations differ depending on their valence state and size (in comparison to the Zr^{4+}). Oversized Y^{3+} (1.019 Å) contribute to the stabilization by two mechanisms, first generating oxygen ion vacancies associated to the Zr cations, and second by expanding the cation lattice. These both decrease the oxygen "overcrowding" around the zirconium cations. Doping Ce^{4+} (having the same valence state as zirconium cation) does not (theoretically) create any oxygen vacancies. The stabilizing effect of oversized Ce^{4+} (0.97 Å) is thus the result of dilating the cation network reducing the "overcrowding" [61–64]. This is why the stabilizing efficiency of Y^{3+} is reported to be higher than Ce^{4+} [16], and as observed here to give similar stabilization effect for half the amount.

From the horizontal axes of the diagrams, for a porous system the critical $YO_{1.5}$ content to achieve the tetragonal phase in a $YO_{1.5}$-doped zirconia is concluded to be approximately 4.5, 4.9 and 5 mol% for heat treating temperatures of 1150, 1350 and 1500°C, respectively. The corresponding values for a dense form are approximately 3.9, 3.9, and 4.1. By defining the stabilizing ratio of $YO_{1.5}$ to CeO_2 stabilizers as *S* (equals to the slope of the dashed and solid lines), an effective amount of critical stabilizer in terms of $YO_{1.5}$ can be expressed as:

$$(YO_{1.5})_{cr}^{eff} = YO_{1.5}\ (mol\%) + CeO_2\ (mol\%)/S \qquad (8)$$

where *S* varies slightly with sintering temperature and density.

3.5. Grain growth in the sintered pellets

Figure 6shows the microstructure of pellets prepared from CHFS, Cerpotech and Tosoh powders sintered at 1150 and 1500°C. The average grain sizes and densities of the samples are presented in Figure 7a. For the samples sintered at 1150°C, the 5Ce 2Y-SZ and 4Y-SZ compounds have close average grain sizes (127 and 139 nm, respectively) while the 2.5Ce 2.5Y-SZ compound has a larger average grain size (180 nm). The grain size distribution of these samples (sintered at 1150°C) is shown in Figure 7b. The largest grains in 4Y-SZ and 5Ce 2Y-SZ pellets are around 250 nm. As the two pellets were fully tetragonal (Table 3), it can be concluded that the critical grain size for the tetragonal to monoclinic phase transformation on cooling for the 4Y-SZ and 5Ce 2Y-SZ compounds at the measured densities is above 250 nm.

The 2.5Ce 2.5Y-SZ pellet had only 30.2 % tetragonal phase. Its grain size distribution shows that 30.2 % of grains have a size of less than 140 nm. Therefore, one can estimate the 140 nm as a critical grain size for the tetragonal to monoclinic phase transformation for the 2.5Ce 2.5Y-SZ ceramic at the density of 81 %. This is significantly smaller than the 250 nm grain size discussed before. As a result, even if the 2.5Ce 2.5Y-SZ pellet had a similar grain size distribution as the 4Y-SZ and 5Ce 2Y-SZ pellets, it would not be fully tetragonal after being sintered at 1150°C. This suggests that although the samples sintered at different temperatures have slightly different grain size

distributions and densities, it is still possible to consider their phase compositions to specify the stability regions where a full stabilization of the tetragonal phase is expected.

At 1500°C, the 2.5Ce 2.5Y-SZ and 5Ce 2Y-SZ pellets have close grain size distributions and densities (Figure 7a), despite the latter containing pure tetragonal phase while the former having 67.6 % of the monoclinic phase. This confirms the chief effect of stabilizer concentration in stabilizing the tetragonal phase, where a slight change of stabilizer content change significantly the stability behavior.

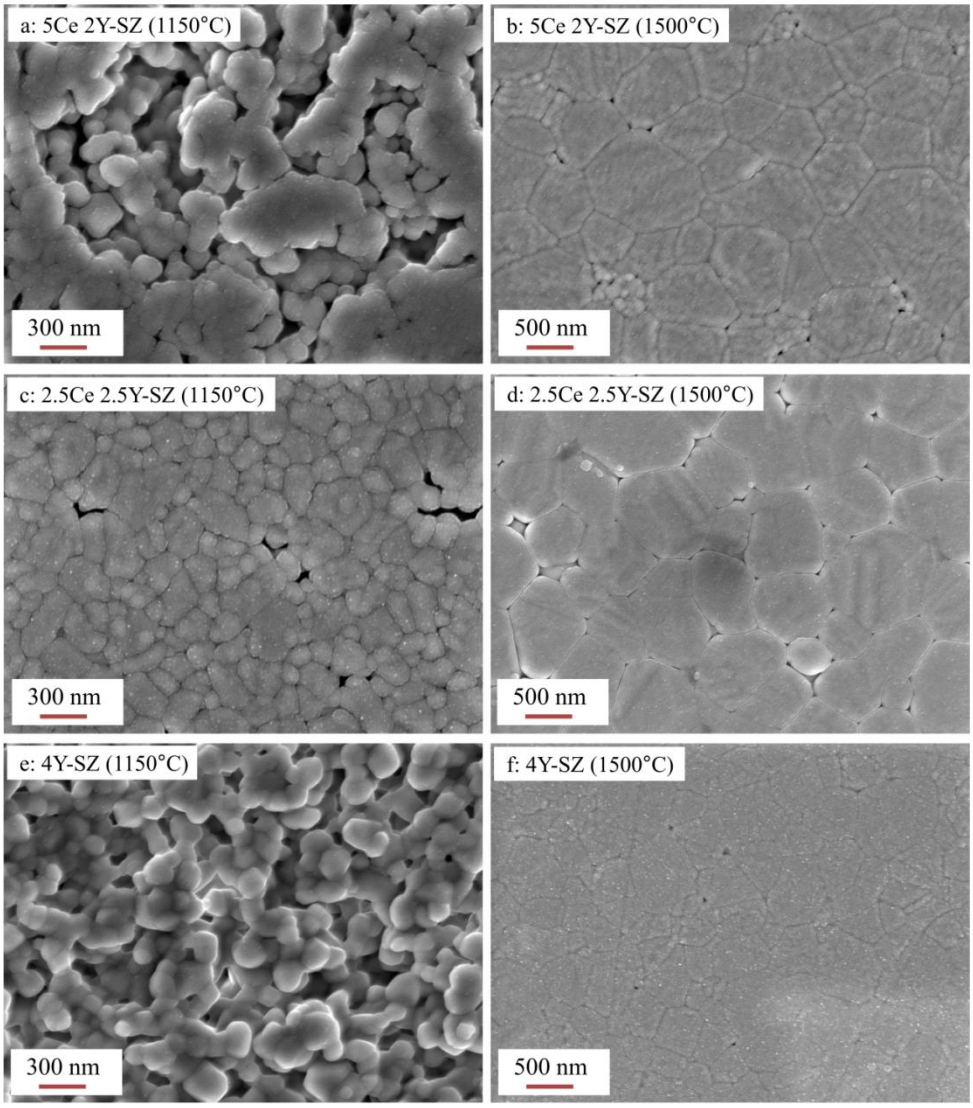

Figure 6: SEM images of 5Ce 2Y-SZ, 2.5Ce 2.5Y-SZ and 4Y-SZ pellets sintered at 1150 and 1500°C.

As discussed earlier, the stability of the tetragonal phase requires the grain size of zirconia to remain below the critical size for the tetragonal to monoclinic phase transformation. Grain growth is dependent on several parameters, including the sintering method, heat-treatment profile (i.e. ramp rate and dwell time) and characteristics of the initial powder/green ceramic (particle size distribution, agglomeration, morphology, density etc.). This may explain the variation of the phase stability results in literature. For instance, Bravo-Leon and co-workers [26] obtained a fully tetragonal ceramic in 1.5 mol% $YO_{1.5}$ doped zirconia (1.5YSZ) sintered at 1175°C for 5 h, while Trunec and co-workers [65]

concluded the 1100°C as the maximum sintering temperature to avoid the tetragonal to monoclinic phase transformation in 1.5YSZ. Thus, definitive transformation boundaries can hardly be drawn due to the differences in characteristics of starting powders, ceramic processing techniques and sintering profiles.

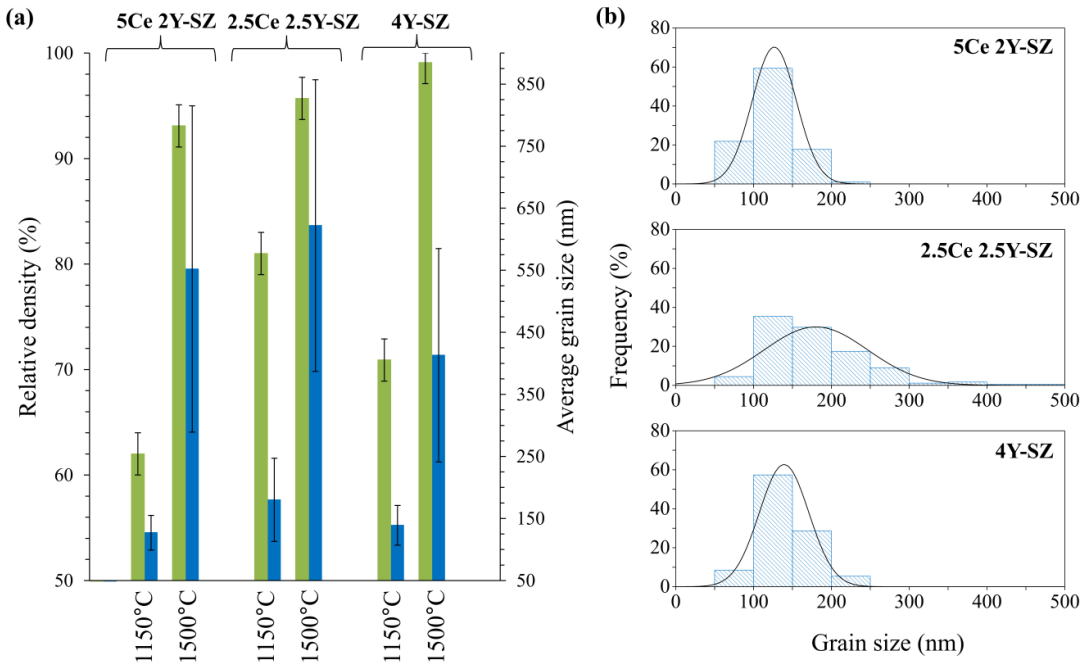

Figure 7: (a) Average grain size (blue bars) and density (green bars) of 5Ce 2Y-SZ, 2.5Ce 2.5Y-SZ and 4Y-SZ pellets sintered at 1150 and 1500°C, (b) grain size distribution of the pellets sintered at 1150°C.

In this study, we processed nanometric powders using conventional sintering and a relatively common heat-treatment profile. The phase composition and grain size distribution analyses confirmed that the results can be appropriately used to develop phase transformation maps. Therefore, although this is not to be considered as definitive transformation boundary diagrams, the results of this study can be applied as a processing guide for stabilizer selection in Ce-Y co-doped zirconia ceramics while using nanometric powders and conventional sintering.

4. Conclusions

The stability of the tetragonal phase in Ce-Y co-doped nanocrystalline zirconia heat-treated at 1150, 1350 and 1500°C was studied in this work. To elucidate the effect of particle packing (density) on the phase stability, samples were investigated in the form of both powders and pellets and the results were used to construct phase transformation boundaries for both systems. The developed diagrams present the compositional region of suitable stabilizer amounts resulting in a balanced stability and transformability of the tetragonal zirconia. It is further concluded that:

- $YO_{1.5}$ and CeO_2 supplement each other in stabilizing the tetragonal phase, and for a porous system $YO_{1.5}$ can, to achieve similar stability, be replaced with *S*-times the amount of CeO_2. For the porous samples *S* was found to be equal to 2 for all the heat treatment temperatures. For materials in dense form the *S* values are 2.1, 2.4, and 2.35 for heat treatment temperatures of 1150, 1350, and 1500°C, respectively.
- Simplifying above summarized findings; as a rule of thumb, the stabilizing effect of $YO_{1.5}$ can be considered twice that of CeO_2.
- For calcined powders, $(YO_{1.5})_{cr}^{eff}$ is 4.5, 4.9 and 5 mol% when sintering at 1150, 1350 and 1500°C, respectively. In a dense system the corresponding values are 3.9, 3.9, and 4.1 mol%.
- The critical amount of stabilizer needed to stabilize a dense system is thus *ca.* 10 – 20 % smaller than in a porous system. This should be borne in mind when designing the processing conditions for porous bodies.
- Continuous hydrothermal flow synthesis was found to be a suitable method to synthesize fine, monodispersed Ce-Y co-doped particles. The synthesized particles had an average crystallite size of 7 to 8.5 nm and were all fully tetragonal.

Supporting Information description

The refined lattice parameters of the 5.5Ce 2.5Y-SZ powder as well as the calculated interplanar spacing of the crystal planes for the as-synthesized and calcined (at 1500°C) samples.

Acknowledgement

This work has been part of the SYNFUEL (sustainable synthetic fuels from biomass gasification and electrolysis) project. The authors would like to thank Innovation fund, Denmark, for the financial support of the project (File No. 4106-00006B).

References

[1] J. Chevalier, J. Loh, L. Gremillard, S. Meille, E. Adolfson, Low-temperature degradation in zirconia with a porous surface, Acta Biomater. 7 (2011) 2986–2993.

[2] T. Klemensø, D. Boccaccini, K. Brodersen, H.L. Frandsen, P. V. Hendriksen, Development of a novel ceramic support layer for planar solid oxide cells, Fuel Cells. 14 (2014) 153–161.

[3] I. Denry, J.R. Kelly, State of the art of zirconia for dental applications, Dent. Mater. 24 (2008) 299–307.

[4] J.R. Kelly, I. Denry, Stabilized zirconia as a structural ceramic: An overview, Dent. Mater. 24 (2008) 289–298.

[5] J.A. Escribano, J. García-Fayos, J.M. Serra, Shaping of 3YSZ porous substrates for oxygen separation membranes, J. Eur. Ceram. Soc. 37 (2017) 5223–5231.

[6] D.W. Ni, B. Charlas, K. Kwok, T.T. Molla, P.V. Hendriksen, H.L. Frandsen, Influence of temperature and atmosphere on the strength and elastic modulus of solid oxide fuel cell anode supports, J. Power Sources. 311 (2016) 1–12.

[7] Y.Y. Huang, T.J. McCarthy, W.M.H. Sachtler, Preparation and catalytic testing of mesoporous sulfated zirconium dioxide with partially tetragonal wall structure, Appl. Catal. A Gen. 148 (1996) 135–154.

[8] S. Shukla, S. Seal, Thermodynamic Tetragonal Phase Stability in Sol−Gel Derived Nanodomains of Pure Zirconia, J. Phys. Chem. B. 108 (2004) 3395–3399.

[9] P. Khajavi, A.A. Babaluo, A. Tavakoli, A. Mirzaei, Stabilization of the metastable tetragonal phase in zirconia nanopowders synthesized via polyacrylamide gel method, Ind. Eng. Chem. Res. 53 (2014) 164–172.

[10] J.A. Wang, M.A. Valenzuela, J. Salmones, A. Vázquez, A. García-Ruiz, X. Bokhimi, Comparative study of nanocrystalline zirconia prepared by precipitation and sol-gel methods, Catal. Today. 68 (2001) 21–30.

[11] J. Liang, X. Jiang, G. Liu, Z. Deng, J. Zhuang, F. Li, Y. Li, Characterization and synthesis of pure ZrO_2 nanopowders via sonochemical method, Mater. Res. Bull. 38 (2003) 161–168.

[12] T. Chraska, A.H. King, C.C. Berndt, On the size-dependent phase transformation in nanoparticulate zirconia, Mater. Sci. Eng. A. 286 (2000) 169–178.

[13] R.H.J. Hannink, P.M. Kelly, B.C. Muddle, Transformation Toughening in Zirconia-Containing Ceramics, J. Am. Ceram. Soc. 83 (2004) 461–487.

[14] K. Tsukuma, M. Shimada, Strength, fracture toughness and Vickers hardness of CeO_2-stabilized tetragonal ZrO_2 polycrystals (Ce-TZP), J. Mater. Sci. 20 (1985) 1178–1184.

[15] T.K. Gupta, F.F. Lange, J.H. Bechtold, Effect of stress-induced phase transformation on the properties of polycrystalline zirconia containing metastable tetragonal phase, J. Mater. Sci. 13 (1978) 1464–1470.

[16] J. Chevalier, L. Gremillard, A. V. Virkar, D.R. Clarke, The tetragonal-monoclinic transformation in zirconia: Lessons learned and future trends, J. Am. Ceram. Soc. 92 (2009) 1901–1920.

[17] P. Khajavi, A.A. Babaluo, Preparation of non-permselective sulfated zirconia catalytic membrane for use in a catalytic membrane reactor, Chem. Eng. Res. Des. 104 (2015) 472–478.

[18] I. Nettleship, R. Stevens, Tetragonal zirconia polycrystal (TZP)-A review, Int. J. High Technol. Ceram. 3 (1987) 1–32.

[19] J. Eichler, M. Hoffman, U. Eisele, J. Rödel, R-curve behaviour of 2Y-TZP with submicron grain size, J. Eur. Ceram. Soc. 26 (2006) 3575–3582.

[20] P. Duran, M. Gonzalez, C. Moure, J.R. Jurado, C. Pascual, A new tentative phase equilibrium diagram for the ZrO_2-CeO_2 system in air, J. Mater. Sci. 25 (1990) 5001–5006.

[21] G.S.A.M. Theunissen, J.S. Bouma, a. J. a. Winnubst, a. J. Burggraaf, Mechanical properties of ultra-fine grained zirconia ceramics, J. Mater. Sci. 27 (1992) 4429–4438.

[22] B. Basu, Toughening of yttria-stabilised tetragonal zirconia ceramics, Int. Mater. Rev. 50 (2005) 239–256.

[23] F.F. Lange, Transformation toughening - Part 3 Experimenta observations in the ZrO_2- Y_2O_3 system, J. Mater. Sci. 17 (1982) 240–246.

[24] D.N. Boccaccini, H.L. Frandsen, S. Soprani, M. Cannio, T. Klemensø, V. Gil, P.V. Hendriksen, Influence of porosity on mechanical properties of tetragonal stabilized zirconia, J. Eur. Ceram. Soc. (2017).

[25] M. Trunec, Z. Chlup, Higher fracture toughness of tetragonal zirconia ceramics through nanocrystalline structure, Scr. Mater. 61 (2009) 56–59.

[26] A. Bravo-Leon, Y. Morikawa, M. Kawahara, M.J. Mayo, Fracture toughness of nanocrystallien tetragonal zirconia with low ytttia content, Acta Mater. 50 (2002) 4555–4562.

[27] B.A. Cottom, M.J. Mayo, Fracture toughness of nanocrystalline ZrO_2-3mol% Y_2O_3 determined by vickers indentation, Scr. Mater. 34 (1996) 809–814.

[28] S. Maschio, O. Sbaizero, S. Meriani, Mechanical properties in the ceria-zirconia system, J. Eur. Ceram. Soc. 9 (1992) 127–132.

[29] J.G. Duh, J.U. Wan, Developments in highly toughened CeO_2-Y_2O_3-ZrO_2 ceramic system, J. Mater. Sci. 27 (1992) 6197–6203.

[30] J.G. Duh, M.Y. Lee, Fabrication and sinterability in Y_2O_3-CeO_2-ZrO_2, J. Mater. Sci. 24 (1989) 4467–4474.

[31] J. Duh, H. Dai, B. Chiou, Sintering, Microstructure, Hardness, and Fracture Toughness Behavior of Y_2O_3-CeO_2-ZrO_2, J. Am. Ceram. Soc. 71 (1988) 813–819.

[32] G.S.A.M. Theunissen, A.J.A. Winnubst, A.J. Burggraaf, Effect of dopants on the sintering behaviour and stability of tetragonal zirconia ceramics, J. Eur. Ceram. Soc. 9 (1992) 251–263.

[33] J. Lin, J. Duh, Correlation of mechanical properties and composition in tetragonal CeO_2–Y_2O_3–ZrO_2 ceramic system, Mater. Chem. Phys. 78 (2002) 246–252.

[34] J.-D. Lin, J.G. Duh, Mechanical properties and resistance to hydrothermal aging of ceria-and yttria-doped tetragonal zirconia ceramics, Mater. Chem. Phys. 77 (2003) 808–818.

[35] J. Lin, J. Duh, Fracture toughness and hardness of ceria-and yttria-doped tetragonal zirconia ceramics, Mater. Chem. Phys. 78 (2003) 253–261.

[36] S.G. Huang, J. Vleugels, L. Li, O. Van der Biest, P.L. Wang, Composition design and mechanical properties of mixed (Ce,Y)-TZP ceramics obtained from coated starting powders, J. Eur. Ceram. Soc. 25 (2005) 3109–3115.

[37] M. Hayakawa, Y. Inoue, M. Oka, H. Nakagawa, Martensitic Transformation and Mechanical Properties of (Y, Ce)-Tetragonal Zirconia Polycrystals, Mater. Trans. JIM. 36 (1995) 729–734.

[38] H. Yokokawa, N. Sakai, T. Horita, K. Yamaji, Y. Xiong, T. Otake, H. Yugami, T. Kawada, J. Mizusaki, Phase diagram calculations of ZrO_2-based ceramics with an emphasis on the reduction/oxidation equilibria of cerium ions in the ZrO_2-$YO_{1.5}$-CeO_2-$CeO_{1.5}$ system, J. Phase Equilibria. 22 (2001) 331–338.

[39] L. Li, B.O. Van Der, W.P. L., V. J., C.W. W., H.S. G., Estimation of the phase diagram for the ZrO_2–Y_2O_3–CeO_2 system, J. Eur. Ceram. Soc. 21 (2001) 2903–2910.

[40] P.R. Prezas, M.J. Soares, F.N.A. Freire, M.P.F. Graça, Structural , electrical and dielectric characterization of TeO_2–WO_3–Y_2O_3–Er_2O_3–Yb_2O_3 glasses, J. Eur. Ceram. Soc. 68 (2015) 314–319.

[41] M. Yashima, H. Takashina, M. Kakihana, M. Yoshimura, low-Temperature Phase Equilibriaby the Flux Method and the Metastable-Stable Phase Diagram in the ZrO_2-CeO_2 System, J. Am. Ceram. Soc. 77 (1994) 1869–1874.

[42] J.W. Drazin, R.H.R. Castro, Phase stability in nanocrystals: A predictive diagram for yttria-zirconia, J. Am. Ceram. Soc. 98 (2015) 1377–1384.

[43] M. Asadikiya, H. Sabarou, M. Chen, Y. Zhong, Phase diagram for a nano-yttria-stabilized zirconia system, RSC Adv. 6 (2016) 17438–17445.

[44] P. Zielke, Y. Xu, S.B. Simonsen, P. Norby, R. Kiebach, Simulation, design and proof-of-concept of a two-stage continuous hydrothermal flow synthesis reactor for synthesis of functionalized nano-sized inorganic composite materials, J. Supercrit. Fluids. 117 (2016) 1–12.

[45] H. Toraya, M. Yoshimura, S. Somiya, Calibration Curve for Quantitative Analysis of the Monoclinic-Tetragonal ZrO_2 System by X-Ray Diffraction, Commun. Am. Ceram. Soc. 67 (1984) C119–C121.

[46] H.P. Klug, L.E. Alexander, X-Ray Diffraction Procedures: For Polycrystalline and Amorphous Materials, 2nd ed., Wiley, 1974.

[47] H.M. Rietveld, A profile refinement method for nuclear and magnetic structures, J. Appl. Crystallogr. 2 (1969) 65–71.

[48] R.J. Hill, C.J. Howard, A Computer Program for Rietveld Analysis of Fixed-wavelength X-ray and Neutron Powder Diffraction Patterns AAEC (Now ANSTO) Rep. M112, Lucas Heights Research Laboratory, Australia, 1986.

[49] S. Brunauer, P.H. Emmett, E. Teller, Adsorption of Gases in Multimolecular Layers, J. Am. Chem. Soc. 60 (1938) 309–319.

[50] P. Bowen, Particle size distribution measurement from millimeters to nanometers and from rods to platelets, J. Dispers. Sci. Technol. 23 (2002) 631–662.

[51] A. Chatterjee, S.K. Pradhan, A. Datta, M. De, D. Chakravorty, Stability of cubic phase in nanocrystalline ZrO_2, J. Mater. Res. 9 (1994) 263–265.

[52] S. Roy, J. Ghose, Synthesis of stable nanocrystalline cubic zirconia, Mater. Res. Bull. 35 (2000) 1195–1203.

[53] D.G. Lamas, A.M. Rosso, M.S. Anzorena, A. Fernández, M.G. Bellino, M.D. Cabezas, N.E. Walsöe de Reca, A.F. Craievich, Crystal structure of pure ZrO_2 nanopowders, Scr. Mater. 55 (2006) 553–556.

[54] S. Tsunekawa, S. Ito, Y. Kawazoe, J.T. Wang, Critical size of the phase transition from cubic to tetragonal in pure zirconia nanoparticles, Nano Lett. 3 (2003) 871–875.

[55] S. Manna, T. Ghoshal, A.K. Deb, S.K. De, Structural stability and optical properties of nanocrystalline zirconia, J. Appl. Crystallogr. 43 (2010) 780–789.

[56] R.C. Garvie, Stabilization of the tetragonal structure in zirconia microcrystals, J. Phys. Chem. 82 (1978) 218–224.

[57] F.F. Lange, Transformation toughening-Part 1 Size effects associated with the thermodynamics of constrained transformations, J. Mater. Sci. 17 (1982) 225–234.

[58] A. Suresh, M.J. Mayo, W.D. Porter, Thermodynamics of the tetragonal-to-monoclinic phase transformation in fine and nanocrystalline yttria-stabilized zirconia powders, J. Mater. Res. 18 (2003) 2912–2921.

[59] A. Suresh, M.J. Mayo, W.D. Porter, C.J. Rawn, Crystallite and grain-size-dependent phase transformations in yttria-doped zirconia, J. Am. Ceram. Soc. 86 (2003) 360–362.

[60] F.F. Lange, Transformation toughening-Part 3 Experimental observations in the ZrO_2-Y_2O_3 system, J. Mater. Sci. 17 (1982) 240–246.

[61] P. Li, I.-W. Chen, J.E. Penner-Hahn, Effect of Dopants on Zirconia Stabilization—An X-ray Absorption Study: I, Trivalent Dopants, J. Am. Ceram. Soc. 77 (1994) 118–128.

[62] P. Li, I.-W. Chen, J.E. Penner-Hahn, Effect of Dopants on Zirconia Stabilization—An X-ray Absorption Study: II, Tetravalent dopants, J. Am. Ceram. Soc. 77 (1994) 1281–1288.

[63] S. Shukla, S. Seal, Mechanisms of room temperature metastable tetragonal phase stabilisation in zirconia, Int. Mater. Rev. 50 (2005) 45–64.

[64] J. Chevalier, L. Gremillard, Zirconia as a Biomaterial, in: Compr. Biomater. II, 2017: pp. 122–144.

[65] M. Trunec, K. Maca, Z. Shen, Warm pressing of zirconia nanoparticles by the spark plasma sintering technique, Scr. Mater. 59 (2008) 23–26.

Supporting Information

Table S1. Refined lattice parameters of the as-synthesized and calcined 5.5Ce 2.5Y-SZ powder (Numbers in parenthesis indicate the estimated standard deviations)

	As-synthesized	**Calcined at 1500°C**
***a* (Å)**	3.613 (2)	3.6147 (9)
***c* (Å)**	5.1918 (5)	5.1999 (2)

Table S2. Interplanar spacing of different planes in as-synthesized and calcined 5.5Ce 2.5Y-SZ powder (calculated using the refined lattice parameters)

Planes (hkl)			**d (Å)**	
h	**k**	**l**	**As-synthesized**	**Calcined at 1500°C**
1	0	1	2.966	2.968
0	0	2	2.596	2.600
1	1	0	2.555	2.556
1	0	2	2.108	2.111
1	1	2	1.821	1.823
2	0	0	1.806	1.807
2	0	1	1.706	1.707
1	0	3	1.561	1.563
2	1	1	1.543	1.544
2	0	2	1.483	1.484
2	1	2	1.372	1.373
0	0	4	1.298	1.300
2	2	0	1.277	1.278
1	0	4	1.222	1.223
2	1	3	1.181	1.182
3	0	1	1.173	1.174
1	1	4	1.157	1.159
2	2	2	1.146	1.147
3	1	0	1.143	1.143